A General Approach to Convert Hemicyanine Dyes into Highly Optimized Photoacoustic Scaffolds for Analyte Sensing

Sarah H Gardner†[a], Catharine J Brady†[b], Cameron Keeton[b], Anuj K Yadav [b], Sharath C Mallojjala[c], Melissa Y Lucero[b], Shengzhang Su[b], Zhengxin Yu[b], Jennifer S Hirschi[c], Liviu M Mirica[b], Jefferson Chan*[a,b]

† These authors contributed equally

[a] SH Gardner, Prof. J Chan
Department of Biochemistry
University of Illinois at Urbana−Champaign
Urbana, Illinois 61801, United States
E-mail: jeffchan@illinois.edu

[b] SH Gardner, CJ Brady, C Keeton, Dr. AK Yadav, MY Lucero, S Su, Z Yu, Prof. LM Mirica, Prof. J Chan
Department of Chemistry and Beckman Institute for Advanced Science and Technology
University of Illinois at Urbana−Champaign
Urbana, Illinois 61801, United States

[c] Dr. SC Mallojjala, Prof. JS Hirschi
Department of Chemistry
Binghamton University
Binghamton, New York 13902, United States

Supporting information for this article is given via a link at the end of the document.

Abstract: In the context of deep-tissue disease biomarker detection and analyte sensing of biologically relevant species, the impact of photoacoustic imaging has been profound. However, most photoacoustic imaging agents to date are based on the repurposing of existing fluorescent dye platforms that exhibit non-optimal properties for photoacoustic applications (e.g., high fluorescence quantum yield). Herein, we introduce two effective modifications to the hemicyanine dye to afford PA-HD, a new dye scaffold optimized for photoacoustic probe development. We observed a significant increase in the photoacoustic output, representing an increase in sensitivity of 4.8-fold and a red-shift of the λ_{abs} from 690 nm to 745 nm to enable ratiometric imaging. Moreover, to demonstrate the generalizability and utility of our remodeling efforts, we developed three probes using common analyte-responsive triggers for beta-galactosidase activity (PA-HD-Gal), nitroreductase activity (PA-HD-NTR), and hydrogen peroxide (PA-HD-H_2O_2). The performance of each probe (responsiveness, selectivity) was evaluated *in vitro* and *in cellulo*. To showcase the enhance properties afforded by PA-HD for *in vivo* photoacoustic imaging, we employed an Alzheimer's disease model to detect H_2O_2. In particular, the photoacoustic signal at 735 nm in the brains of 5xFAD mice (a murine model of Alzheimer's disease) increased by 1.79 ± 0.20-fold relative to background indicating the presence of oxidative stress, whereas the change in wildtype mice was negligible (1.02 ± 0.14). These results were confirmed via ratiometric calibration which was not possible using the parent HD platform.

Introduction

Photoacoustic imaging is a powerful *in vivo* approach that is characterized by the generation of ultrasound waves which result from the excitation of an optical absorber with light.[1, 2] In theory, any light-absorbing material can be induced to afford a photoacoustic readout; however, in practice, only molecules with a wavelength of maximum absorbance in the near-infrared (NIR) region (λ_{abs} > 650 nm), a high extinction coefficient ($\epsilon > 10^4$ $M^{-1}cm^{-1}$) and a low quantum yield (Φ < 5%) are desirable. Initially, when photoacoustic imaging emerged as an *in vivo* biomedical technique, various endogenous absorbers such as hemoglobin, oxyhemoglobin, and melanin were exploited to provide contrast. These studies set the stage for label-free imaging of various cancer types and inflammatory conditions in human patients.[3] However, as the demand for improved performance, better contrast, greater target specificity, and molecular information grew, efforts turned toward the design of targeted contrast agents[4] and activatable photoacoustic probes (also known as acoustogenic probes)[5, 6] to reliably identify diseased tissue and to monitor biological analytes, respectively.

Owing to the intrinsic similarities between photoacoustic and fluorescence imaging (i.e., the requirement of light excitation), it is reasonable that most photoacoustic imaging agents to date have relied heavily on the repurposing of existing fluorophores. For example, indocyanine green (ICG), an FDA-approved cyanine-based fluorescent dye, was utilized extensively in early studies for contrast-enhanced photoacoustic imaging even though it is prone to photobleaching and oxidative decomposition. Likewise, the first small-molecule activatable photoacoustic probe (designed to detect Cu^{2+})[7] was based on the aza-BODIPY dye, which is another NIR fluorescent platform.[8] Subsequent studies have resulted in a palette of aza-BODIPY-based photoacoustic probes for hypoxia,[9-11] nitric oxide,[12-14] peroxynitrite,[15] hydrogen peroxide,[16] pH,[17] redox status,[18] and photodynamic therapy.[19, 20] In addition, our group put forth significant efforts to optimize this scaffold for photoacoustic imaging; however, this required the handling of unstable species such as reactive azirine intermediates, as well as challenging (and sometimes low yielding) purifications to separate the desired heteropyrrole coupling product from the unwanted symmetrical aza-BODIPYs.[21]

Due to these limitations, our design has not yet been widely adopted by other probe developers. Beyond aza-BODIPYs, other NIR fluorescent platforms such as cyanines[22-30] and hemicyanine dyes (HD)[31-39] have also been repurposed extensively (Scheme 1a).

HDs have attracted considerable attention from the field owing to their ease of synthesis (one-step starting from a parent cyanine and resorcinol) and the presence of a convenient handle (i.e., -OH or -NH_2) from which analyte-responsive triggers can be appended to.[40] Unfortunately, HDs are far from ideal for photoacoustic analyte sensing. First, the λ_{abs} of a 'capped' probe (~600) typically falls below the NIR cutoff of 650 nm, as well as the lower wavelength limit of our commercial photoacoustic imaging systems (660 nm (MSOT iNVision, iThera) and 680 nm (Nexus 128+, Endra)). These constraints preclude ratiometric calibration which can account for imaging artifacts that result from photobleaching or differential probe clearance. Second, HDs are highly fluorescent molecules (Φ = ~30-40%), meaning less of the excited state will relax via non-radiative decay to afford a photoacoustic signal. In this study, we introduce two highly effective modifications to transform existing HD designs into optimized scaffolds for photoacoustic imaging by substituting the endocyclic oxygen with a sulfur moiety and by tuning the phenolic pKa value (herein referred to as PA-HDs). To demonstrate generalizability, we prepared three enhanced photoacoustic probes from PA-HD for β-galactosidase activity, nitroreductase activity, and hydrogen peroxide (H_2O_2). Beyond cellular studies in which all three probes were tested, we also employed our H_2O_2 probe to image oxidative stress in a murine model of Alzheimer's disease.

Results and Discussion

The design of PA-HD is based on the premise that sulfur-substitution can potentially red-shift the λ_{abs} value by up to 50 nm and thus, can facilitate deeper tissue imaging and ratiometric calibration. Moreover, we anticipate two additional benefits from this modification that favor photoacoustic imaging. First, we hypothesized the fluorescent quantum yield will be attenuated and second, we expected the extinction coefficient to be enhanced. It is noteworthy that although the apparent pKa of regular HDs (herein referred to as O-HD) was reported to be ~5.6,[40] this value appears to be inaccurate. In our hands we measured a value of 7.5 (Figure S1). This discrepancy likely resulted because the pH of each buffer system used to construct the corresponding pH-profile was not adjusted after the organic co-solvent component was added. A high pKa value will decrease the photoacoustic sensitivity and lead to imaging artifacts since the protonated form of O-HD will have a similar absorbance to that of the unactivated probe. Therefore, in addition to performing the proposed O to S substitution, it is critical to install an ortho chloro group to lower the phenolic pKa which ensures that upon unmasking of the trigger, the turned over PA-HD will exist predominantly in a deprotonated form. To this end, we synthesized PA-HD by first substituting the *meso*-chloro group of Cy7-Cl with thiophenol **1** to furnish cyanine **2** in 52% yield. This intermediate was then demethylated with BBr_3 and heated under basic conditions after solvent exchange to initiate the retro-Knoevenagel reaction to generate **PA-HD** in 64% yield over 2-steps (33% overall yield).

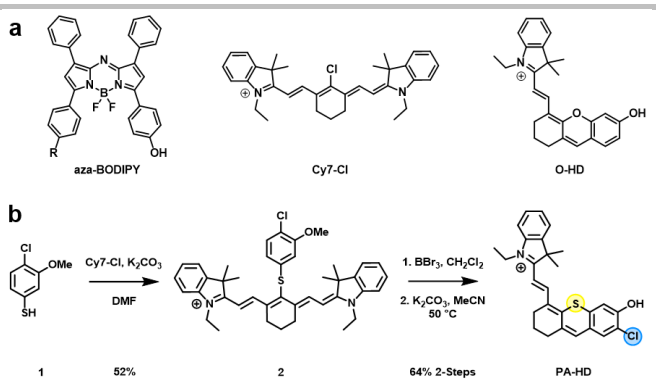

Scheme 1. a) Examples of NIR fluorescent dyes that have been repurposed for photoacoustic applications. b) Synthesis of PA-HD.

With PA-HD in hand, we first determined that the λ_{abs} was positioned at 745 nm which represents a bathochromic shift of 55 nm relative to O-HD (Figure 1a). Moreover, it is apparent that at pH 7.4, over half the population of O-HD is protonated and this results in a blue-shifted λ_{abs} and low ϵ. In contrast, since the apparent pKa value of PA-HD is 6.0, over 96% of the dye will be deprotonated at physiological pH (Figure S2). We also found that the ϵ had increased significantly by 62% from 8.2 × 10^4 $M^{-1}cm^{-1}$ to 13.3 × 10^4 $M^{-1}cm^{-1}$ and that the Φ decreased by six-fold from 30% to 5%. As mentioned previously, meeting these two design criteria will translate into enhanced photoacoustic properties. To evaluate

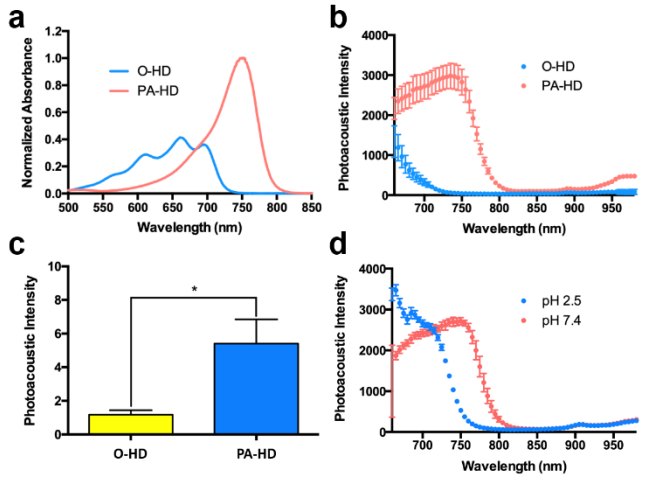

Figure 1. a) Absorbance and b) PA spectra of O-HD and PA-HD at pH 7.4 (1:1 v/v PBS:EtOH). Dye concentration was 25 μM for each dye. c) Normalized photoacoustic intensity of O-HD and PA-HD in a tissue phantom containing 60% milk to mimic scattering effects in dense tissue. [PA-HD] = 0.5 μM (*n* = 3). Statistical analysis was performed using two-tailed Student's t-test (α = 0.05), *: p < 0.05. d) Photoacoustic spectra of PA-HD at pH 2.5 and 7.4.

the impact of sulfur-substitution with respect to the photoacoustic signal intensity and potential ratiometric sensing capabilities, we conducted a series of head-to-head *in vitro* experiments. First, we embedded solutions of each dye (25 μM) in an agar-based tissue phantom (10% milk) and obtained photoacoustic spectra over a wavelength range of 660 to 980 nm (Figure 1b). While the O-HD λ_{abs} clearly fell outside the NIR window, the highest intensity for PA-HD was centered at ~735 nm. This represents a 4.8-fold increase in sensitivity when comparing the highest signals.

Additionally, we show a dose-dependent increase in the photoacoustic intensity after correcting for wavelength-dependent differences in fluence (Figure S3). Next, we reduced the dye concentration to 0.5 μM and changed the composition of milk in the phantom to 60% to mimic the scattering effects of dense tissue (e.g., brain). Even under these conditions that are designed to attenuate the photoacoustic signal, we could readily detect PA-HD but not O-HD (Figure S4). The corresponding normalized photoacoustic intensities (relative to background) were 5.4 ± 2.5-fold and 1.18 ± 0.47-fold, respectively (Figure 1c). To evaluate the potential of this new scaffold for ratiometric imaging, we subjected PA-HD to acidic conditions since protonation of the phenol is an effective proxy for the presence of a trigger at this position. Indeed, the protonated form of PA-HD exhibits a λ_{abs} at 650 nm (Figure S5). The ratios of the deprotonated and protonated forms at 650 nm and 745 nm based on absorbance were found to be 0.36 and 16.81, respectively (Figure 1d). This represents a theoretical turn-on response of 46.7 (defined as $ratio_{745}/ratio_{650}$). Similar results were obtained when the experiment was performed at 660 nm (lower wavelength limit) and 735 nm (maximum signal) via photoacoustic imaging to give a turn-on response of 3.7. Together these results demonstrate PA-HD can be employed for ratiometric imaging, while this is not possible with O-HD.

Next, we converted PA-HD into a series of three activatable photoacoustic probes to demonstrate that the enhanced properties afforded by the sulfur-substitution are generalizable. Specifically, PA-HD-Gal (Figure 2a), PA-HD-NTR (Figure 2c), and PA-HD-H_2O_2 (Figure 2e) were developed for β-galactosidase activity, nitroreductase activity, and H_2O_2, respectively. We selected these three imaging targets because their corresponding triggers are commonly employed to validate new dye systems and they are important in a host of physiological and pathological processes. For instance, β-galactosidase expression has been used as a marker to identify senescent cells[41] and ovarian cancer.[42] Nitroreductase has been used as a target to detect gram positive and negative bacteria,[43] as well as tumor hypoxia since it is overexpressed in many cancer types.[44] Lastly, H_2O_2 is not only an important signaling molecule, at elevated levels it is a general indicator of oxidative stress in a variety of disease states.[45]

After synthesizing the three probes, each was subjected to *in vitro* testing to assess target-responsiveness. We found that PA-HD-Gal was readily activated upon incubation with recombinant beta-galactosidase. Specifically, a dose-dependent (0 to 10 U/mL) change in the absorbance (shift of the λ_{abs} from 640 to 745 nm) was observed, representing a maximum signal enhancement of 9.1 ± 0.5-fold based on absorbance (Figure 2b). We confirmed that this increase was due to the enzyme target because heat-inactivation of beta-galactosidase prior to incubation with PA-HD-Gal completely attenuated probe activation (Figure S6). Likewise, PA-HD-NTR was activated by recombinant nitroreductase from *E. coli* (19.8 ±1.7-fold change in fluorescence after 1 h). Moreover, the trigger was demonstrated to be stable in the presence of biological thiols such as Cys, H_2S, and GSH which can potentially reduce the nitro group and lead to 1,4-elimination to give a false response (Figure 2d).[46] Finally, we determined that PA-HD-H_2O_2 retained its responsiveness to H_2O_2. Specifically, a 6.3 ± 0.8-fold and 11.9 ± 1.5-fold change in fluorescence was noted after incubation of the probe for 1 h with 100 μM and 500 μM H_2O_2, respectively (Figure 2f). In contrast, when PA-HD-H_2O_2 was subjected to selectivity screening against a panel of reactive oxygen/nitrogen species (hypochlorite, nitric oxide, tert-butyl hydroperoxide, superoxide, peroxynitrite) there was no significant turn-on. Collectively, these results show that installation of established triggers onto our new photoacoustic scaffold does not impact their performance. Additional *in vitro* characterization can be found in the supporting information document and the photophysical properties of all dyes are summarized below in Table 1.

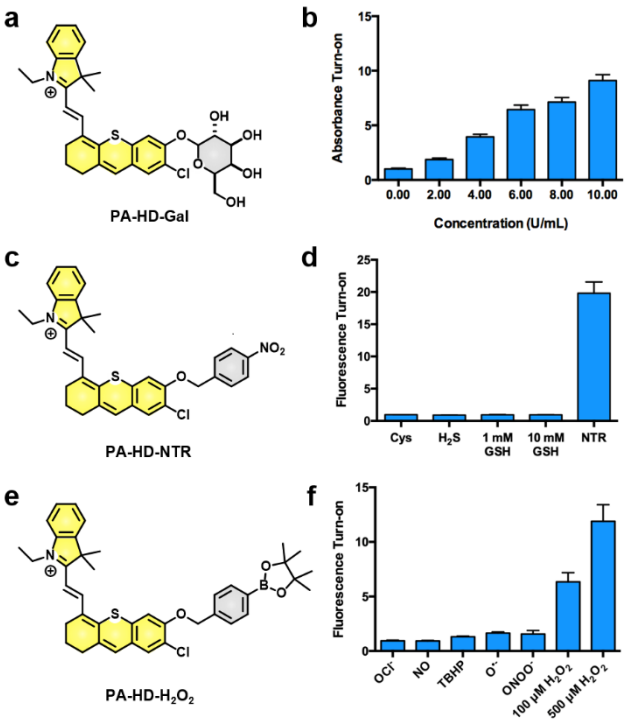

Figure 2. a) Chemical structure of PA-HD-Gal. b) Dose-dependent response of 5 μM PA-HD-Gal after 1 h to 0, 2, 4, 6, 8, or 10 U/mL of *E. Coli* beta-galactosidase at pH 7.4 (9:1 v/v PBS:MeCN) (Mean ± SD, *n* = 5). c) Chemical structure of PA-HD-NTR. d) Response of 2 μM PA-HD-NTR to biologically relevant thiols (Cys and H_2S 100 μM) and GSH at 1 mM and 10 mM for 15 min at pH 7.4 (9:1 v/v PBS:MeCN) (Mean ± SD, *n* = 3). Complete activation mediated by 2 U/mL *E. coli* nitroreductase. e) Chemical structure of PA-HD-H_2O_2. f) Response of 2 μM PA-HD-H_2O_2 to OCl^-, NO, TBHP, O_2^-, $ONOO^-$ (100 μM) and H_2O_2 (100 μM and 500 μM) for 1 h at pH 7.4 (9:1 v/v PBS:MeCN) (Mean ± SD, *n* = 3).

Table 1. Summary of photophysical properties

Compound	λ_{abs}[a] (nm)	λ_{em}[a] (nm)	ϵ[a] (10^4 $M^{-1}cm^{-1}$)	ϕ_F [a,b] (%)	PABF (10^4)	pKa[c]
O-HD	690	712	8.2	30	5.7	7.5
PA-HD	745	765	13.3	5	12.6	6.0
PA-HD-Gal	640	728	3.8	0.7	3.8	N.D.
PA-HD-NTR	642	735	2.7	0.7	2.8	N.D.
PA-HD-H_2O_2	645	738	2.8	0.7	2.7	N.D.

a] Determined at pH 8.25 in 1:1 v/v PBS:MeOH. [b] vs. ICG in DMSO. [c] pKa values determined in 1:1 v/v Britton–Robinson buffers ranging from pH 2.6 to 11.3. N.D. = Not determinable.

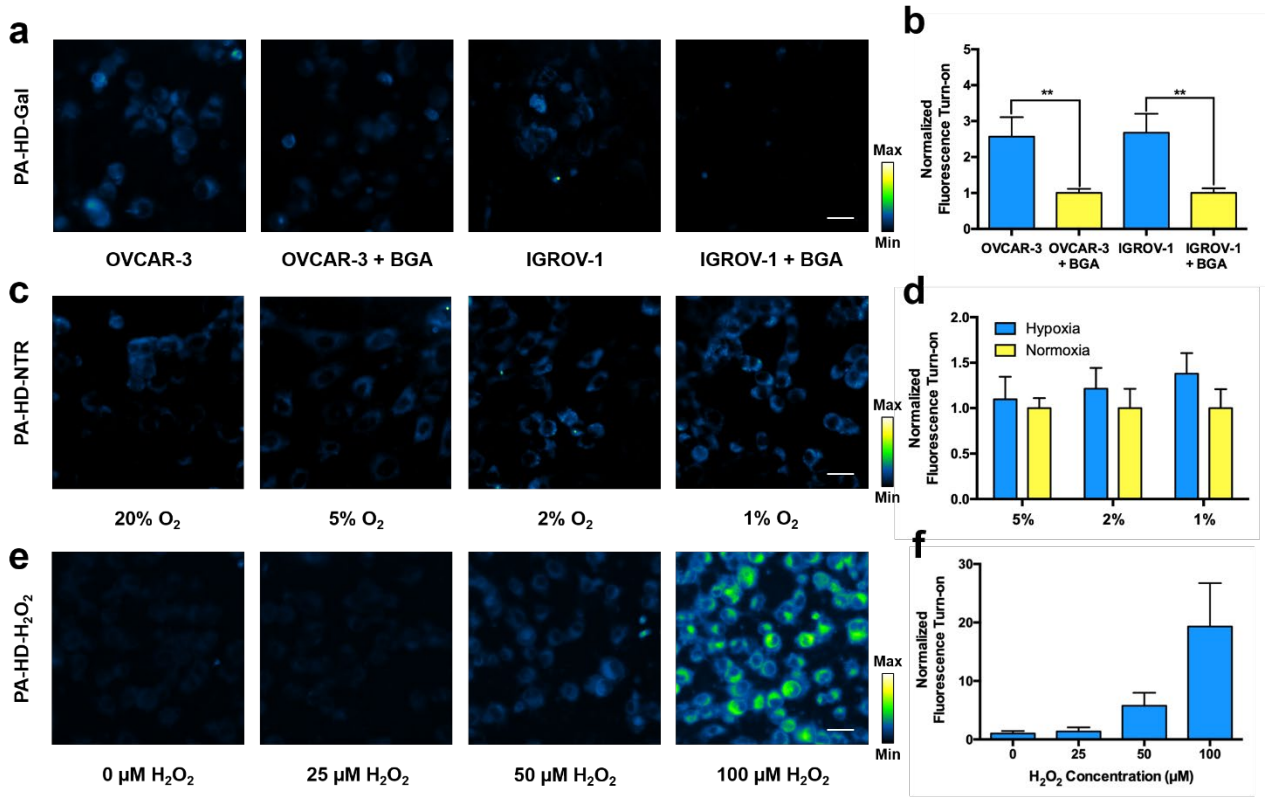

Figure 3. a) Fluorescent images of PA-HD-Gal (4 μM) in ovarian cancer cell lines (OVCAR-3 and IGROV-1) pre-treated with a vehicle control or BGA, a beta-galactosidase inhibitor (1.5mM). *n* = 3 for each condition. Statistical analysis was performed using two-tailed Student's t-test (α = 0.05), **: $p < 0.01$. b) Quantified data from a) normalized to inhibitor condition. c) Fluorescent images of PA-HD-NTR (2 μM) in ID8 cells cultured under the indicated oxygen atmosphere (20,5, 2, or 1 % oxygen). *n* = 3 for each condition. d) Quantified data from c) normalized to a normoxic control. e) Fluorescent Images of PA-HD-H_2O_2 (10 μM) in NeuroScreen-1 cells treated with various concentrations of H_2O_2 (0, 25, 50 100 μM). *n* = 3 for each condition. f) Quantified data from e) normalized to the 0 μM H_2O_2 condition.

We utilized the MTT assay to evaluate cytotoxicity of PA-HD in several mammalian cell lines. Incubation of PA-HD for 6 h at concentrations up to 10 μM did not significantly impact cell viability (Figure S7). With these results in hand, we focused our attention on evaluating the performance of each probe in cell-based studies. Beta-galactosidase is known to be expressed in ovarian cancer presumably because it is involved in the processing of glycans such as sialyl Lewis x.[47] Upon incubation of two human ovarian cancer cell lines, OVCAR-3 and IGROV-1, with PA-HD-Gal we were able to observe an apparent cytosolic staining pattern which suggests our probe was being activated by beta-galactosidase (Figure 3a). To confirm these results, we prepared BGA, a potent beta-galactosidase inhibitor,[48] to determine whether pretreatment would attenuate probe activation. Relative to OVCAR-3 and IGROV-1 cells that were not treated with the inhibitor, the signal intensity was 2.18-fold and 2.78-fold lower, respectively (Figure 3b). Next, the ability of PA-HD-NTR to distinguish between normoxic and hypoxic conditions via nitroreductase activity was tested. 4T1 breast cancer cells were cultured in a 20%, 5%, 2%, or 1% oxygen atmospheres for ~12 h before treatment with PA-HD-NTR. Under oxygen deficient conditions, nitroreductases present within cells can convert the aryl nitro group to the corresponding hydroxyl amine or amino moieties via multiple single electron transfer events. This reduction can facilitate unmasking of PA-HD via self-immolative chemistry. As anticipated, the signal was barely discernable from background when PA-HD-NTR was incubated under normoxic conditions (20% O_2) (Figure 3c). In contrast, the intensity was 1.38 ± 0.10-fold higher at 1% oxygen (Figure 3d). Importantly, the low but statistically significant signal enhancement is a consequence of the trigger which requires chronic hypoxic conditions to upregulate nitroreductase expression. Finally, NeuroScreen-1 cells, a model system for neurons, was stained with PA-HD-H_2O_2 and treated with 0, 25, 50, or 100 μM H_2O_2 (Figure 3e). We selected this cell line because oxidative stress plays a central role in neurodegenerative diseases, as well as aging of the brain. Our results revealed a dose-dependent increase in the signal intensity where the highest concentration of H_2O_2 resulted in a 19.3 ± 7.4-fold turn-on response after incubation (Figure 3f).

Finally, it is critical for us to evaluate whether the enhanced photoacoustic properties of PA-HD will effectively translate in a deep-tissue context. Owing to its excellent analyte selectivity profile and ability to detect H_2O_2 in a dose-dependent manner, we sought to employ PA-HD-H_2O_2 to image oxidative stress (via H_2O_2 detection) in an Alzheimer's disease model. The brain consumes massive amounts of oxygen to fuel its stringent metabolic demands.[49] However, when the natural antioxidant defense systems of the brain are compromised, a net increase in the generation of reactive oxygen species will result. Since oxidative stress is a hallmark of many neurological disorders including Alzheimer's disease,[50] it is reasonable to assume that H_2O_2 will be elevated in the brain; however, there is limited direct evidence showing this to be true at the molecular level.[51, 52] In our study, we systemically administered PA-HD-H_2O_2 to 5xFAD mice which is a well-establish transgenic model engineered to express the human amyloid beta protein precursor.[53] We employed photoacoustic imaging at 660 nm to track probe uptake and observed a signal

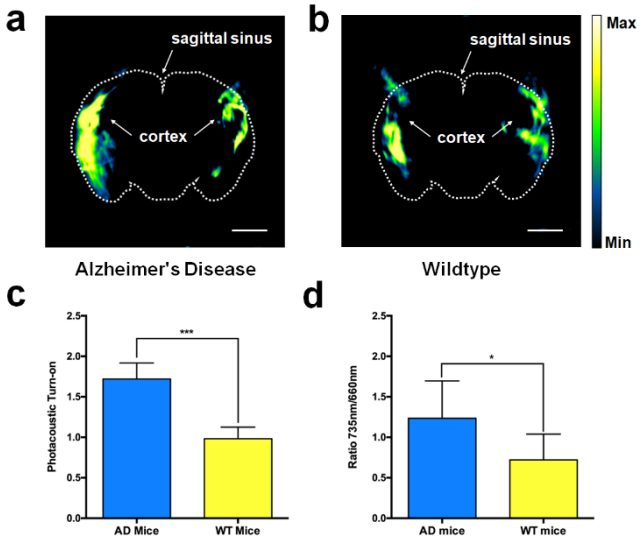

Figure 4. Representative photoacoustic images of the brain from a) an Alzheimer's disease mouse and b) a wildtype mouse captured 2.5 h after PA-HD-H_2O_2 was administered via retroorbital injection with excitation provided at 735 nm. Scale bar represents 2.5 mm. Dotted white outline of the brain is for visualization purposes only. Brain region cropped and overlayed onto a dark background. c) Photoacoustic turn-on response for Alzheimer's disease mice (n = 5) and wildtype mice (n = 6). Error bars = SD. Statistical analysis was performed using two-tailed Student's t-test (α = 0.05), ***: $p < 0.001$. d) Photoacoustic ratio at 735 nm/660 nm of data from c). Statistical analysis was performed using the Mann-Whitney U test

increase at this wavelength that plateaued after ~1 h. To ensure sufficient time for probe activation, we waited a total of 2.5 h before irradiating the brain at 735 nm to detect the turned over product. A marked increase in the photoacoustic signal at this wavelength relative to the initial timepoint was observed (1.79 ± 0.20-fold increase) indicating conversion of PA-HD-H_2O_2 to PA-HD. In contrast, the turn-on response for healthy wildtype controls (B6SJLF1/J mice) was only 1.02 ± 0.14-fold. To corroborate these results, we turned to ratiometric analysis. We hypothesized the PA_{735}/PA_{660} ratio will be higher in the 5xFAD mice compared to the B6SJLF1/J mice at the 2.5 h timepoint since this would represent probe activation and generation of PA-HD. Indeed, the ratio for the 5xFAD mice was 1.23 ± 0.46, whereas the ratio for the B6SJLF1/J mice was 0.85 ± 0.07. Ratiometric imaging would not have possible with O-HD.

Conclusion

At the onset of this study, our goal was to establish a new dye platform that is optimized for the development of activatable photoacoustic probes. This approach represents a significant departure from the common practice of repurposing NIR fluorescent dyes that exhibit sub-optimal properties for photoacoustic imaging. One of the key criteria that we prioritized when developing PA-HD was accessibility, since we believe a high synthetic overhead (~ eight steps) would be less desirable to probe developers in the field. The O-HD dye developed by Lin and co-workers represents an attractive starting point for our remodelling efforts because it can be prepared from Cy7-Cl and resorcinol in a single step and has been shown to be a versatile platform for various biological applications. Beginning from 4-chloro-3-methoxybenzenethiol, PA-HD can be prepared in only three-steps with an overall yield of 33.3%. In this study, we demonstrated that substitution of the endocyclic oxygen atom with a sulfur group affords many desired properties. For instance, we observed a red-shifted λ_{abs} of 55 nm which facilitated access to deeper tissue and enabled ratiometric imaging. The ability to confirm an *in vivo* imaging result by tracking the signal change at two wavelengths clearly sets PA-HD apart from O-HD. While spectral unmixing is another strategy we could have potentially utilized to isolate the signal of PA-HD-H_2O_2 from that of background, this requires us to obtain a high-quality *in vivo* spectrum of the probe which we were unable to do in this instance. This highlights why ratiometric imaging is so critical. It is noteworthy that while we were evaluating the photoacoustic properties of PA-HD, a group prepared a NIR fluorescent probe based on a similar platform (lacking the *ortho*-chloro group) to image cysteine in live cells.[54] However, as we have demonstrated in this work, sulfur-substitution results in a significant decrease in the fluorescent quantum yield which favors photoacoustic imaging while rendering the dye less effective for optical imaging. Indeed, to acquire the fluorescent cell images featured in Figure 3, it was necessary for us to irradiate with the LED light source set at 100% power in some instances. With this in mind, we envision PA-HD will facilitate the development of a diverse range of new activatable photoacoustic probes. We are optimistic that PA-HD will become widely adopted by the photoacoustic field and this work will result in a divergence between O-HD-based probes for fluorescent applications and PA-HD-based chemical tools for photoacoustic imaging.

Acknowledgements

The authors acknowledge the National Institutes of Health for support (R35GM133581 to J.C.; R01GM114588 to L.M.M.). This work used the XSEDE computational resource which is supported by National Science Foundation grant number ACI-1548562 allocation TG-CHE180061. C.J.B. acknowledges the Chemistry-Biology Interface Training Grant (T32-GM136629) and Robert C. and Carolyn J. Springborn Graduate Fellowship for support. M.Y.L. thanks the Alfred P. Sloan Foundation for financial support. Major funding for the 500 MHz Bruker CryoProbeTM was provided by the Roy J. Carver Charitable Trust (Muscatine, Iowa; Grant No. 15-4521) to the School of Chemical Sciences NMR Lab. The Q-Tof Ultima mass spectrometer was purchased in part with a grant from the National Science Foundation, Division of Biological Infrastructure (DBI-0100085). We also thank Prof. Erik R. Nelson (Molecular and Integrative Physiology, UIUC) for ID8 and IGROV-1 cells and Prof. Kai Zhang (Biochemistry, UIUC) for NeuroScreen-1 cells. Furthermore, we thank Dr. Sandy McMasters (UIUC Cell Media Facility) for help with preparation of cell culture media and technical expertise and Dr. Andrew Brannen (iThera Medical) for helpful suggestions.

Keywords: Photoacoustic imaging • Acoustogenic Probe • Analyte Sensing • Hydrogen Peroxide • Alzheimer's Disease

[1] Wang, L. V., and Hu, S. (2012) Photoacoustic Tomography: In Vivo Imaging from Organelles to Organs, *Science 335*, 1458.
[2] Yadav, A. K., Hernandez, S., Su, S., and Chan, J. (2020) Acoustic-based chemical tools for profiling the tumor microenvironment, *Current Opinion in Chemical Biology 57*, 114-121.
[3] Steinberg, I., Huland, D. M., Vermesh, O., Frostig, H. E., Tummers, W. S., and Gambhir, S. S. (2019) Photoacoustic clinical imaging, *Photoacoustics 14*, 77-98.
[4] Weber, J., Beard, P. C., and Bohndiek, S. E. (2016) Contrast agents for molecular photoacoustic imaging, *Nature Methods 13*, 639-650.
[5] Reinhardt, C. J., and Chan, J. (2018) Development of Photoacoustic Probes for in Vivo Molecular Imaging, *Biochemistry 57*, 194-199.
[6] Knox, H. J., and Chan, J. (2018) Acoustogenic Probes: A New Frontier in Photoacoustic Imaging, *Accounts of Chemical Research 51*, 2897-2905.
[7] Li, H., Zhang, P., Smaga, L. P., Hoffman, R. A., and Chan, J. (2015) Photoacoustic Probes for Ratiometric Imaging of Copper(II), *Journal of the American Chemical Society 137*, 15628-15631.
[8] Ge, Y., and O'Shea, D. F. (2016) Azadipyrromethenes: from traditional dye chemistry to leading edge applications, *Chemical Society Reviews 45*, 3846-3864.
[9] Knox, H. J., Hedhli, J., Kim, T. W., Khalili, K., Dobrucki, L. W., and Chan, J. (2017) A bioreducible N-oxide-based probe for photoacoustic imaging of hypoxia, *Nature Communications 8*, 1794.
[10] Knox, H. J., Kim, T. W., Zhu, Z., and Chan, J. (2018) Photophysical Tuning of N-Oxide-Based Probes Enables Ratiometric Photoacoustic Imaging of Tumor Hypoxia, *ACS Chemical Biology 13*, 1838-1843.
[11] Chen, M., Knox, H. J., Tang, Y., Liu, W., Nie, L., Chan, J., and Yao, J. (2019) Simultaneous photoacoustic imaging of intravascular and tissue oxygenation, *Opt. Lett. 44*, 3773-3776.
[12] Reinhardt, C. J., Zhou, E. Y., Jorgensen, M. D., Partipilo, G., and Chan, J. (2018) A Ratiometric Acoustogenic Probe for in Vivo Imaging of Endogenous Nitric Oxide, *Journal of the American Chemical Society 140*, 1011-1018.
[13] Zhou, E. Y., Knox, H. J., Reinhardt, C. J., Partipilo, G., Nilges, M. J., and Chan, J. (2018) Near-Infrared Photoactivatable Nitric Oxide Donors with Integrated Photoacoustic Monitoring, *Journal of the American Chemical Society 140*, 11686-11697.
[14] Reinhardt, C. J., Xu, R., and Chan, J. (2020) Nitric oxide imaging in cancer enabled by steric relaxation of a photoacoustic probe platform, *Chemical Science 11*, 1587-1592.
[15] Zhang, J., Zhen, X., Upputuri, P. K., Pramanik, M., Chen, P., and Pu, K. (2017) Activatable Photoacoustic Nanoprobes for In Vivo Ratiometric Imaging of Peroxynitrite, *Advanced Materials 29*, 1604764.
[16] Lu, X., Zhao, M., Chen, P., Fan, Q., Wang, W., and Huang, W. (2018) Enhancing hydrophilicity of photoacoustic probes for effective ratiometric imaging of hydrogen peroxide, *Journal of Materials Chemistry B 6*, 4531-4538.
[17] Geng, J., Li, W., Smaga, L. P., Sottos, N. R., and Chan, J. (2018) Damage-Responsive Microcapsules for Amplified Photoacoustic Detection of Microcracks in Polymers, *Chemistry of Materials 30*, 2198-2202.
[18] Zheng, J., Zeng, Q., Zhang, R., Xing, D., and Zhang, T. (2019) Dynamic-Reversible Photoacoustic Probe for Continuous Ratiometric Sensing and Imaging of Redox Status in Vivo, *Journal of the American Chemical Society 141*, 19226-19230.
[19] Tang, Q., Si, W., Huang, C., Ding, K., Huang, W., Chen, P., Zhang, Q., and Dong, X. (2017) An aza-BODIPY photosensitizer for photoacoustic and photothermal imaging guided dual modal cancer phototherapy, *Journal of Materials Chemistry B 5*, 1566-1573.
[20] Gawale, Y., Adarsh, N., Kalva, S. K., Joseph, J., Pramanik, M., Ramaiah, D., and Sekar, N. (2017) Carbazole-Linked Near-Infrared Aza-BODIPY Dyes as Triplet Sensitizers and Photoacoustic Contrast Agents for Deep-Tissue Imaging, *Chemistry – A European Journal 23*, 6570-6578.
[21] Zhou, E. Y., Knox, H. J., Liu, C., Zhao, W., and Chan, J. (2019) A Conformationally Restricted Aza-BODIPY Platform for Stimulus-Responsive Probes with Enhanced Photoacoustic Properties, *Journal of the American Chemical Society 141*, 17601-17609.
[22] Mishra, A., Jiang, Y., Roberts, S., Ntziachristos, V., and Westmeyer, G. G. (2016) Near-Infrared Photoacoustic Imaging Probe Responsive to Calcium, *Analytical Chemistry 88*, 10785-10789.
[23] Zhang, J., Smaga, L. P., Satyavolu, N. S. R., Chan, J., and Lu, Y. (2017) DNA Aptamer-Based Activatable Probes for Photoacoustic Imaging in Living Mice, *Journal of the American Chemical Society 139*, 17225-17228.
[24] Roberts, S., Seeger, M., Jiang, Y., Mishra, A., Sigmund, F., Stelzl, A., Lauri, A., Symvoulidis, P., Rolbieski, H., Preller, M., Deán-Ben, X. L., Razansky, D., Orschmann, T., Desbordes, S. C., Vetschera, P., Bach, T., Ntziachristos, V., and Westmeyer, G. G. (2018) Calcium Sensor for Photoacoustic Imaging, *Journal of the American Chemical Society 140*, 2718-2721.
[25] Xiao, H., Wu, C., Li, P., Gao, W., Zhang, W., Zhang, W., Tong, L., and Tang, B. (2017) Ratiometric photoacoustic imaging of endoplasmic reticulum polarity in injured liver tissues of diabetic mice, *Chemical Science 8*, 7025-7030.
[26] Liu, Y., Wang, S., Ma, Y., Lin, J., Wang, H.-Y., Gu, Y., Chen, X., and Huang, P. (2017) Ratiometric Photoacoustic Molecular Imaging for Methylmercury Detection in Living Subjects, *Advanced Materials 29*, 1606129.
[27] Ma, G., Gao, X., Jiang, C., Xing, S., Wei, C., Huang, P., and Lin, J. (2019) pH-Responsive Nanoprobe for In Vivo Photoacoustic Imaging of Gastric Acid, *Analytical Chemistry 91*, 13570-13575.
[28] Zhang, Y., He, S., Chen, W., Liu, Y., Zhang, X., Miao, Q., and Pu, K. (2021) Activatable Polymeric Nanoprobe for Near-Infrared Fluorescence and Photoacoustic Imaging of T Lymphocytes, *Angewandte Chemie International Edition 60*, 5921-5927.
[29] Meng, X., Zhang, J., Sun, Z., Zhou, L., Deng, G., Li, S., Li, W., Gong, P., and Cai, L. (2018) Hypoxia-triggered single molecule probe for high-contrast NIR II/PA tumor imaging and robust photothermal therapy, *Theranostics 8*, 6025-6034.
[30] Zhang, C., Gao, R., Zhang, L., Liu, C., Yang, Z., and Zhao, S. (2020) Design and Synthesis of a Ratiometric Photoacoustic Probe for In Situ Imaging of Zinc Ions in Deep Tissue In Vivo, *Analytical Chemistry 92*, 6382-6390.
[31] Wu, Y., Huang, S., Wang, J., Sun, L., Zeng, F., and Wu, S. (2018) Activatable probes for diagnosing and positioning liver injury and metastatic tumors by multispectral optoacoustic tomography, *Nature Communications 9*, 3983.
[32] Sun, L., Wu, Y., Chen, J., Zhong, J., Zeng, F., and Wu, S. (2019) A Turn-On Optoacoustic Probe for Imaging Metformin-Induced Upregulation of Hepatic Hydrogen Sulfide and Subsequent Liver Injury, *Theranostics 9*, 77-89.
[33] Ma, T., Zheng, J., Zhang, T., and Xing, D. (2018) Ratiometric photoacoustic nanoprobes for monitoring and imaging of hydrogen sulfide in vivo, *Nanoscale 10*, 13462-13470.
[34] Cheng, P., Chen, W., Li, S., He, S., Miao, Q., and Pu, K. (2020) Fluoro-Photoacoustic Polymeric Renal Reporter for Real-Time Dual Imaging of Acute Kidney Injury, *Advanced Materials 32*, 1908530.
[35] Gao, W., Li, X., Liu, Z., Fu, W., Sun, Y., Cao, W., Tong, L., and Tang, B. (2019) A Redox-Responsive Self-Assembled Nanoprobe for Photoacoustic Inflammation Imaging to Assess Atherosclerotic Plaque Vulnerability, *Analytical Chemistry 91*, 1150-1156.
[36] Zeng, Q., Wu, Y., and Zhang, T. (2019) Photoacoustic nanoprobe for β-galactosidase activity detection and imaging in vivo, *Journal of Innovative Optical Health Sciences 12*, 1941001.
[37] Gao, X., Ma, G., Jiang, C., Zeng, L., Jiang, S., Huang, P., and Lin, J. (2019) In Vivo Near-Infrared Fluorescence and Photoacoustic Dual-Modal Imaging of Endogenous

Alkaline Phosphatase, *Analytical Chemistry 91*, 7112-7117.
[38] Huang, J., Wu, Y., Zeng, F., and Wu, S. (2019) An Activatable Near-Infrared Chromophore for Multispectral Optoacoustic Imaging of Tumor Hypoxia and for Tumor Inhibition, *Theranostics 9*, 7313-7324.
[39] Lucero, M. Y., and Chan, J. (2020) *Towards Personalized Medicine: Photoacoustic Imaging Enables Companion Diagnosis and Targeted Treatment of Lung Cancer*.
[40] Yuan, L., Lin, W., Zhao, S., Gao, W., Chen, B., He, L., and Zhu, S. (2012) A Unique Approach to Development of Near-Infrared Fluorescent Sensors for in Vivo Imaging, *Journal of the American Chemical Society 134*, 13510-13523.
[41] Debacq-Chainiaux, F., Erusalimsky, J. D., Campisi, J., and Toussaint, O. (2009) Protocols to detect senescence-associated beta-galactosidase (SA-βgal) activity, a biomarker of senescent cells in culture and in vivo, *Nature Protocols 4*, 1798-1806.
[42] Asanuma, D., Sakabe, M., Kamiya, M., Yamamoto, K., Hiratake, J., Ogawa, M., Kosaka, N., Choyke, P. L., Nagano, T., Kobayashi, H., and Urano, Y. (2015) Sensitive β-galactosidase-targeting fluorescence probe for visualizing small peritoneal metastatic tumours in vivo, *Nature Communications 6*, 6463.
[43] Wong, R. H. F., Kwong, T., Yau, K.-H., and Au-Yeung, H. Y. (2015) Real time detection of live microbes using a highly sensitive bioluminescent nitroreductase probe, *Chemical Communications 51*, 4440-4442.
[44] Qin, W., Xu, C., Zhao, Y., Yu, C., Shen, S., Lin, L., and Huang, W. (2018) Recent progress in small molecule fluorescent probes for nitroreductase, *Chinese Chemical Letters 29*, 1451-1455.
[45] Iwashita, H., Castillo, E., Messina, M. S., Swanson, R. A., and Chang, C. J. (2021) A tandem activity-based sensing and labeling strategy enables imaging of transcellular hydrogen peroxide signaling, *Proceedings of the National Academy of Sciences 118*, e2018513118.
[46] Montoya, L. A., and Pluth, M. D. (2012) Selective turn-on fluorescent probes for imaging hydrogen sulfide in living cells, *Chemical Communications 48*, 4767-4769.
[47] Saldova, R., Royle, L., Radcliffe, C. M., Abd Hamid, U. M., Evans, R., Arnold, J. N., Banks, R. E., Hutson, R., Harvey, D. J., Antrobus, R., Petrescu, S. M., Dwek, R. A., and Rudd, P. M. (2007) Ovarian Cancer is Associated with Changes in Glycosylation in Both Acute-Phase Proteins and IgG, *Glycobiology 17*, 1344-1356.
[48] Guo, W., Hiratake, J., Ogawa, K., Yamamoto, M., Ma, S. J., and Sakata, K. (2001) Beta-D-glycosylamidines: potent, selective, and easily accessible 1-glycosidase inhibitors, *Bioorg Med Chem Lett 11*, 467-470.
[49] Watts, M. E., Pocock, R., and Claudianos, C. (2018) Brain Energy and Oxygen Metabolism: Emerging Role in Normal Function and Disease, *Frontiers in Molecular Neuroscience 11*.
[50] Huang, W.-J., Zhang, X., and Chen, W.-W. (2016) Role of oxidative stress in Alzheimer's disease, *Biomed Rep 4*, 519-522.
[51] Yang, J., Yang, J., Liang, S. H., Xu, Y., Moore, A., and Ran, C. (2016) Imaging hydrogen peroxide in Alzheimer's disease via cascade signal amplification, *Scientific Reports 6*, 35613.
[52] Yang, J., Zhang, X., Yuan, P., Yang, J., Xu, Y., Grutzendler, J., Shao, Y., Moore, A., and Ran, C. (2017) Oxalate-curcumin–based probe for micro- and macroimaging of reactive oxygen species in Alzheimer's disease, *Proceedings of the National Academy of Sciences 114*, 12384.
[53] Dinkins, M. B., Dasgupta, S., Wang, G., Zhu, G., He, Q., Kong, J. N., and Bieberich, E. (2015) The 5XFAD Mouse Model of Alzheimer's Disease Exhibits an Age-Dependent Increase in Anti-Ceramide IgG and Exogenous Administration of Ceramide Further Increases Anti-Ceramide Titers and Amyloid Plaque Burden, *J Alzheimers Dis 46*, 55-61.
[54] Cai, S., Liu, C., Jiao, X., Zhao, L., and Zeng, X. (2020) A lysosome-targeted near-infrared fluorescent probe for imaging endogenous cysteine (Cys) in living cells, *Journal of Materials Chemistry B 8*, 2269-2274.

Entry for the Table of Contents

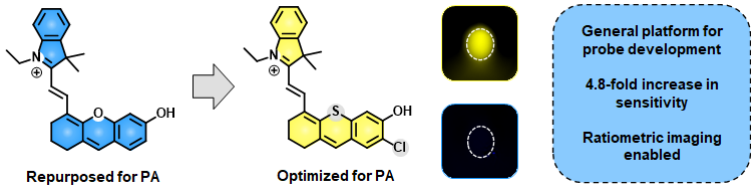

We have developed PA-HD, a new sulfur-substituted dye platform exhibiting enhanced properties for photoacoustic probe development. To demonstrate generalizability, we employed PA-HD to access probes for beta-galactosidase and nitroreductase activities, as well as H_2O_2. Each probe was tested in live cells and *in vivo*. For instance, the H_2O_2 probe was employed to visualized oxidative stress in an Alzheimer's disease model.

Institute and/or researcher Twitter usernames: @ChanLabUIUC @MiricaGroup